Pre-Print Manuscript of Article:
Bridgelall, R., Tolliver, D., Rahman, T., Daleiden, J. F., "Use of Connected Vehicles to Characterize Ride Quality," *Transportation Research Record: Journal of the Transportation Research Board*, Vol. 2589, DOI: 10.3141/2589-13, 2016.

USE OF CONNECTED VEHICLES TO CHARACTERIZE RIDE QUALITY

Raj Bridgelall, Corresponding Author
SMARTSe[SM], Upper Great Plains Transportation Institute
North Dakota State University
P.O. Box 863676, Plano, TX 75086
Phone: (408) 607-3214; Fax: (701) 231-1945; Email: raj.bridgelall@ndsu.edu

Md Tahmidur Rahman
Fugro Roadware, Inc.
8613 Cross Park Drive, Austin, TX 78754
Phone: 512-977-1879; Email: trahman@fugro.com

Denver D. Tolliver
Upper Great Plains Transportation Institute, North Dakota State University
Fargo, ND 58108
Phone: (701) 231-7190; Fax: (701) 231-1945; Email: denver.tolliver@ndsu.edu

Jerome F. Daleiden
Fugro Roadware, Inc.
8613 Cross Park Drive, Austin, TX 78754
Phone: 512-977-1800; Email: jdaleiden@fugro.com

Word count: 5711 + 2 Tables (250 each) + 5 Figures (250 each) = 7461 words

TRR Paper number: 16-0525

Submission Date: February 25, 2016

ABSTRACT
The United States rely on the performance of more than four million miles of roadways to sustain its economic growth and to support the dynamic mobility needs of its growing population. The funding gap to build and maintain roadways is ever widening. Hence, the continuous deterioration of roads from weathering and usage poses significant challenges. Transportation agencies measure ride quality as the primary indicator of roadway performance. The international roughness index is the prevalent measure of ride quality that agencies use to assess and forecast maintenance needs. Most jurisdictions utilize a laser-based inertial profiler to produce the index. However, technical, practical, and budget constraints preclude their use for some facilities, particularly local and unpaved roads that make up more than 90% of the road network in the US. This study expands on previous work that developed a method to transform sensor data from many connected vehicles to characterize ride quality continuously, for all facility types, and at any speed. The case studies used a certified and calibrated inertial profiler to produce the international roughness index. A smartphone aboard the inertial profiler produced simultaneously the roughness index of the connected vehicle method. The results validate the direct proportionality relationship between the inertial profiler and connected vehicle methods within a margin-of-error that diminished below 5% and 2% after 30 and 80 traversal samples, respectively.

INTRODUCTION

Ride quality refers to the degree that a vehicle protects its occupants from factors that decrease ride comfort. The road impact factors (RIF) are uneven surfaces and anomalies such as potholes, cracks, and utility covers. The driver impact factors (DIF) are behaviors such as abrupt braking, rapid acceleration, weaving, and speeding around curves. Hence, the RIF and the DIF can induce motions and noises that cause rider discomfort. The vehicle impact factors (VIF) affect how riders perceive the disturbances from RIF and DIF. The VIF are a strong function of the vehicle suspension and handling characteristics but they can also include other factors such as features of furniture design, interior aesthetics, and entertainment. Altogether, these factors result in the overall ride quality experienced.

Highway agencies narrow the definition of ride quality to the RIF and use a model of the vehicle suspension system, called the Golden Car, to standardize the VIF as a fixed suspension response that dampens vibrations from road roughness (*1*). The Golden Car approximates the suspension response of vehicles typical of the 1980s, which is around the time-period that practitioners agreed on the approach. Nearly all regular passenger and commercial motor vehicles, regardless of their size and weight, provide similar suspension responses because manufacturers design them to attenuate vibrations within a common range of frequencies that cause human discomfort or increase the difficulty of operating vehicles safely (*2*). In particular, humans are most sensitive to vibrations between 4 and 8 Hertz (*3*). For example, the resonant frequency of the human spine is approximately 5 Hertz. The typical suspension system attempts to attenuate vibrations in this frequency range and consequently result in a transfer function that exhibits a sprung- and unsprung-mass resonant mode near 1 and 10 Hertz, respectively (*4*).

The international roughness index (IRI) is currently the prevalent measure of ride quality. Nearly all jurisdictions deploy laser-based inertial profilers to produce the IRI (*5*). The procedure to produce the IRI from elevation profile samples is a mathematical simulation that moves the Golden Car at 80 km/h across the profile. Conversely, the connected vehicle method directly samples the inertial response from many vehicles to produce an average characterization of the ride quality experienced (*6*). In previous work, Bridgelall (2014) proved that the index of roughness derived from connected vehicle sensor data is directly proportional to the IRI (*1*). The inertial sensor used was an industrial grade device that produced high quality accelerometer and global positioning system (GPS) data. Consequently, the proportionality was repeatable within a margin-of-error, in a 95% confidence interval, that was less than 4% after only six traversals.

The objective of this study is to repeat those experiments with a much lower cost inertial and GPS data logger implemented as a smartphone application (app) called PAVVET (*7*). For these experiments, the authors used a certified and calibrated inertial profiler to collect the IRI data. Resource constraints limited the number of traversals available to approximately nine. Hence, the authors utilized a regular sedan to collect PAVVET data from more than 20 traversals across the same route to test the statistical significance and to compare the ride quality characterizations with those using the inertial profiler.

The organization of this paper is as follows: the next section will review the background and models of the IRI and connected vehicle methods of ride quality characterizations to highlight their respective differences. The third section will review the statistical models to transform the connected vehicle data into a single index summary of roughness, and to test its convergence with traversal volume. The fourth section will describe the case studies and discuss the results. The final section will summarize and conclude the study.

RIDE QUALITY CHARACTERIZATIONS

As of 2015, nearly all jurisdictions have begun to use inertial profilers to produce the IRI from samples of the elevation profile (*5*). Although these devices have become the *de facto* method of producing the IRI, technical limitations challenge their use to characterize ride quality for local and unpaved roads (*8*). Such facilities account for more than 90% of the roadways in the U.S. (*9*). In particular, roadway anomalies and the stop-and-go conditions of urban facilities could invalidate miles worth of data collected (*10*). Furthermore, numerous studies demonstrated that the IRI masks road roughness that causes human discomfort (*11*)(*12*)(*13*). Several studies found that the IRI is insensitive to spatial wavelengths that are characteristic of underlying pavement distress symptoms (*14*)(*15*)(*16*)(*17*).

In previous work, Bridgelall (2014) developed a transform to characterize ride quality from the sensor data of connected vehicles (*1*). The result was a road impact factor (RIF) transform that compresses voluminous data from the inertial and geospatial position sensors aboard regular vehicles to produce a single index summary of roughness that is directly proportional to the IRI, at any fixed speed. Unlike the IRI, the RIF-index reflects the actual roughness that users experience when traveling the segment. The RIF-index inherently integrates the average response energy from the combined RIF and VIF of a real vehicle. To remove the wavelength bias that arises from suspension-based mechanical filtering at fixed speeds, the Bridgelall (2014) developed a time-wavelength-intensity-transform (TWIT). This wide-band transform integrates RIF-indices from multiple speed bands to produce a speed-independent and wavelength-unbiased roughness index. Therefore, the TWIT reflects the average roughness experienced for the range of speeds that travelers ride the segment. Averaging the RIF-indices for a given speed band produces a summary of ride quality with ever increasing precision as the number of traversals from connected vehicles increase. The technique is applicable for all facility types, including local and unpaved roads. The IRI requires relatively few traversals to produce an average value with high precision because of its fixed Golden Car parameters and simulation at a fixed speed. Conversely, variations in actual vehicle suspension performance and speed increase the number of traversals needed to provide an equivalent level of precision for RIF-indices.

The International Roughness Index

The definition of the IRI is the accumulated absolute rate difference between the sprung- and unsprung-mass motions of a Golden Car simulated to move at a fixed reference speed (*18*). The notation for the IRI in this development is $I_{\bar{v}}^{L}$ and its definition is

$$I_{\bar{v}}^{L} = \frac{1}{L}\int_{0}^{L/\bar{v}} \left| \dot{z}_s(t) - \dot{z}_u(t) \right| dt \tag{1}$$

where $\dot{z}_s(t)$ and $\dot{z}_u(t)$ are the first derivatives of the Golden Car sprung- and unsprung-mass vertical motions, respectively. The segment length L is typically 500 or 1000 feet. The procedure fixes the speed $\bar{v}$ to the standard reference speed of 80 km/h. Therefore, the IRI ignores any variations in the actual vehicle speed and suspension responses. In fact, some inertial profilers estimate the body bounces of the host vehicle to account for reference plain movements that distort elevation profile measurements. The fixed suspension response of the Golden Car and the fixed reference speed prevents the IRI from reflecting roughness produced from spatial wavelengths that fall outside of a relatively narrow range. Consequently, the IRI cannot reflect

the true roughness that riders experience when traveling a segment at different speeds and in different vehicles.

The Road Impact Factor Transform

The RIF transform integrates the product of the vertical acceleration signal $g_z(t)$ and the longitudinal velocity $v(t)$ such that

$$R_{\bar{v}}^{L} = \sqrt{\frac{1}{L}\int_{0}^{L/\bar{v}} \left| g_z(t) v(t) \right|^2 dt} \tag{2}$$

where the RIF-index $R_{\bar{v}}^{L}$ is the average g-force magnitude experienced per unit of distance L traveled. This expression simply multiplies the vertical acceleration signal from the inertial sensor with the instantaneous velocity, and then accumulates the square of that product across the segment length analyzed. Dividing the accumulated square-of-products by the segment length and then taking the square root yields the RIF-index. For an average speed $v(t) = \bar{v}$, within some speed band across a segment, the RIF-index simplifies to

$$R_{\bar{v}}^{L} = \bar{v}\sqrt{\frac{1}{L}\int_{0}^{L/\bar{v}} \left| g_z(t) \right|^2 dt} = \bar{v}\sqrt{E_{gz}^{L}} \tag{3}$$

where E_{gz}^{L} is the longitudinal energy density of the vertical acceleration signal. The inertial signal energy is in units of joules per meter when the sensor output is in units of volts. The associated discrete time transform is

$$R_{\bar{v}}^{L} = \sqrt{\frac{1}{L}\sum_{n=0}^{N-1} \left| g_{z[n]} v_n \right|^2 \delta t} \tag{4}$$

where the discrete time samples are $t = n \times \delta t$ with sample instant n and average sampling period δt. The inverse of the sampling period is the sample rate of the inertial sensor. The total number of samples is N, therefore, for an average sample interval of δL, the segment length is $N \times \delta L$. Hence, the instantaneous velocity is $v_n = \delta L_n / \delta t_n$ and the discrete time RIF transform simplifies to

$$R_{\bar{v}}^{L} = \sqrt{\frac{1}{N}\sum_{n=0}^{N-1} g_{z[n]}^2 v_n}\,. \tag{5}$$

For a constant velocity v_c, the RIF-index is related to the root-mean-squared (RMS) value of the vertical acceleration signal g_{rms} such that

$$R_{\bar{v}}^{L} = \sqrt{\frac{1}{N}\sum_{n=0}^{N-1} v_n g_{z[n]}^2} = \sqrt{v_c}\sqrt{\frac{1}{N}\sum_{n=0}^{N-1} g_{z[n]}^2} = g_{rms}\sqrt{v_c}\,. \tag{6}$$

It is evident that the RIF-index is zero when the traversal velocity is zero and increases non-linearly with velocity. Previous work that attempted to relate the accelerometer signal to the IRI witnessed a speed dependency but did not establish a mathematical characterization to explain the behavior observed (*19*)(*20*). The inertial signal output g_{rms} is essentially a convolution of the equivalent quarter-car response with the power spectral density of the elevation profile (*1*).

Therefore, a uniform, broadband power spectral density must produce a constant RMS value. Practically, however, the power spectral density of typical roadways diminishes with shorter spatial wavelengths that translate to higher frequencies in the time domain. Therefore, a combined effect of the nonlinear increases in velocity and the decrease in power spectral density of the elevation profile at higher speeds produces a combined stabilization of the RIF-index.

Based on previous work (*21*), Figure 1a plots the simulated Golden Car vertical responses to bump traversals at 7 m s^{-1} and twice that speed. The simulated bump is 5-cm high by 1-m wide. The sprung-mass response (body bounce) at the lower and higher speeds differ substantially (Figure 1a). Hence, this simulation exemplifies the fundamental reason for variations in the RIF- and IRI-transform outputs as a function of traversal speed (Figure 1b). The RIF-transform (Equation 3) associates the RIF-index with any selected speed band whereas the IRI-transform requires a precise speed of 80 km h^{-1}. Consequently, the RIF/IRI ratio is a function of the traversal speed. Therefore, agencies must standardize on the traversal speed selected for a given facility when measuring the RIF-index to estimate the corresponding IRI.

Unlike the IRI, the RIF-index is a transformation of the inertial and velocity data from the response of an actual vehicle traversing the elevation profile at a given average speed and interval of variability. Therefore, the RIF-indices encapsulate all effects from variations in the elevation profile, speed, suspension responses, and vibration modes that are not present in a simulated Golden Car. Averaging the RIF-indices from many vehicles will attenuate independent noise sources from VIF that are not common mode factors from road roughness.

The Ensemble Average RIF

The ensemble average of the RIF-indices (EAR) from N_v traversals across a path of length L is denoted $\overline{R}_{\bar{\bar{v}}}^{L}$ and it is analogous to the average IRI. The EAR-index is

$$\overline{R}_{\bar{\bar{v}}}^{L} = \frac{1}{N_v}\sum_{\rho=1}^{N_v} R_{\bar{v}}^{L}[\rho] \tag{7}$$

where $R_{\bar{v}}^{L}[\rho]$ is the RIF-index from the ρ^{th} traversal of the segment at an average speed of $\bar{v}$, and $\bar{\bar{v}}$ is the batch mean speed from all traversals. In addition to compressing the inertial and position data longitudinally along the traversal direction, the EAR fuses multiple data streams within the same geospatial window of all traversals. Hence, the EAR-index represents a vertical compression of the stack of RIF-indices produced for a segment for some short time-period, for example, a few hours or a few days.

The EAR-index represents the average roughness that the typical vehicle occupant experiences when traveling the segment within a specified interval of speed or a speed band. For example, selecting data streams from vehicle traversals that are within 5 km/h of an average speed of 80 km/h will produce an EAR-index that summarizes roughness from the range of spatial wavelengths that the IRI characterizes. However, producing the EAR-indices for the prevailing average speed of a given facility type, such as the speed limit, would be more practical and meaningful. That is, the EAR-index will characterize ride quality from spatial wavelengths that induce roughness at the prevailing speeds rather than at the IRI reference speed. Monitoring the EAR-index from the same speed band consistently will reflect changes in ride quality that the average user experiences as the road deteriorates over time. The TWIT integrates the EAR-indices from all speed bands to produce a speed-independent and broadband characterization of roughness over time (*21*).

STATISTICAL MODELS

Agencies may elect to measure and associate a calibrated RIF/IRI ratio for designated vehicles by producing the EAR-indices from several traversals of a facility for which a recent IRI value is available. Alternatively, producing the EAR-index from a selected speed band by sampling the traversal data from many vehicles will obviate the need for calibration to account for the VIF of a specific vehicle. Previous studies of the precision bounds of the EAR-index demonstrate that the margin-of-error, within a 95% confidence interval (MOE_{95}), diminishes rapidly after only several hours of data collection from the typical vehicle mix (*22*). The MOE_{95} will diminish to equivalent levels of precision with fewer traversals when using the same vehicle or vehicle type. GIS platforms that incorporate this connected vehicle method could select similar classes of vehicles from the data stream, traveling under similar conditions of weather, regional climate, and facility type to produce EAR-indices that achieve higher precision characterizations with fewer traversals. This section will develop the statistical tests to demonstrate convergence of the RIF/IRI ratios to the expected values of classical parameterized distributions.

Data Distribution

A histogram of the RIF-indices provides a non-parametric description of the indices produced from the traversals of many vehicles. Subsequently, a least squares approximation of classic distributions that best fit the histogram provides a parametric estimate of their expected values to forecast the achievable precision. The case studies of this work use the critical chi-squared values to test the fitted distributions for candidacy as Gaussian and Student-*t* distributions (*23*). The *t*-distribution is practically identical to the Gaussian distribution when the sample size approaches 30.

Chi-squared Testing

The critical chi-squared value "χ^2 Data" is an evaluation of the statistic

$$\chi^2 = \sum_{k=1}^{n} \frac{\left(O_k - E_k\right)^2}{E_k} \tag{8}$$

where O_k are the histogram values observed in bin k and E_k are the corresponding expected values from the hypothesized distribution. The chi-squared distribution value at 5% significance (α = 5%) is the largest value expected with a probability of at most 5%. The chi-squared degrees of freedom (*df*) are one unit less than the number of histogram bins *n*, minus the two independent distribution parameters estimated, namely the amplitude and the mean. Estimation of the standard deviation is dependent on an estimation of the mean; hence, it does not count towards the *df*. Statisticians generally reject a null hypothesis that the data follow a tested distribution if the critical χ^2 value is larger than the chi-square distribution value at 5% significance, or equivalently, if the significance level calculated for the critical χ^2 value is less than 5%.

Margin-of-Error

The interval $\Delta R^L_{1-\alpha}$ is the margin-of-error within a (1-α)% confidence interval (*24*) such that

$$\Delta R_{1-\alpha}^{L} = \pm \frac{\sigma_R^L \times t_{1-\alpha/2,df}}{\sqrt{N_v}} \quad (9)$$

where $t_{1-\alpha/2,df}$ is the *t*-score at (1-α) probability for a normalized cumulative *t*-distribution of *df* degrees of freedom. The standard deviation of the RIF-index is denoted σ_R^L. The ratio of $\Delta R_{1-\alpha}^{L}$ to the EAR-index $\overline{R}_{\bar{v}}^{L}$ is a proportional measure of the data spread as a percentage. For this study, $MOE_{0.95}$ (%) indicates that 95% of the data points are likely to be within that percentage of the EAR-index.

From the classical theory of error propagation (*24*), the standard deviation of the RIF-index, σ_R^L is:

$$\sigma_R^L = \sqrt{\left(\frac{\partial R_{\bar{v}}^L}{\partial \bar{v}}\right)^2 \sigma_{\bar{v}}^2 + \left(\frac{\partial R_{\bar{v}}^L}{\partial E_{gz}^L}\right)^2 Var\left[E_{gz}^L\right] + \left(\frac{\partial R_{\bar{v}}^L}{\partial \bar{v}}\right)\left(\frac{\partial R_{\bar{v}}^L}{\partial E_{gz}^L}\right)\sigma_{\bar{v}E}^2} \quad (10)$$

where $\sigma_{\bar{v}}^2$ is the variance of the batch mean speed within the selected speed band. The covariance of the batch mean speed and the vertical acceleration signal energy is denoted $\sigma_{\bar{v}E}^2$. Evaluating the partial derivatives indicated in Equation (10) yields:

$$\sigma_R^L = \sqrt{\overline{E}_{gz}^L \sigma_{\bar{v}}^2 + \left(\overline{\bar{v}}/2\right)^2 \frac{Var\left[E_{gz}^L\right]}{\overline{E}_{gz}^L} + \left(\overline{\bar{v}}/2\right)\sigma_{\bar{v}E}^2} \quad (11)$$

where $\overline{E}_{gz}^L$ and $\overline{\bar{v}}$ are the means of the vertical acceleration signal energy and the batch mean speed among traversals, respectively. Therefore, the proportional contribution of the velocity variance to the precision dilution in RIF-indices η_{vR}^L is

$$\eta_{vR}^L = \overline{E}_{gz}^L \left(\frac{\sigma_{\bar{v}}}{\sigma_R^L}\right)^2 \quad (12)$$

RESULTS AND DISCUSSIONS

This section describes the case studies conducted, the method of data processing, and the results obtained from the field experiments. The final section tests the distribution of the RIF/IRI ratios against the classical parameterized distributions to demonstrate convergence with their expected values.

The Case Study Setting

The three pavement sections analyzed are along the frontage road sections of TX-130 (Figure 2a), which is about 20 miles northeast of Austin, Texas. Each test site is a 1000-ft (304.8 meter) section of asphalt pavement. The inertial profiler traversed each segment at approximately 72 km h^{-1} (45 MPH) and 97 km h^{-1} (60 MPH) to observe any differences in each set of roughness indices produced.

The IRI Data Collection and Processing

This study used a calibrated and certified Ames Engineering Model 8300 inertial profiler (Figure 2b). The host vehicle is a Ford E150 XLT Wagon. The ProQual software processed the elevation profile samples to produce indices for the left wheel path (LWP) and right wheel path (RWP) height sensors (*25*). The silver colored line of duct tape across the pavement (Figure 2b) automatically triggers the start of IRI data collection for the inertial profiler. The IRI values utilized for this analysis are the mean values of the LWP and RWP indices.

The RIF Data Collection and Processing

The PAVVET data logger produced samples of the tri-axial acceleration, orientation, velocity, time, and geospatial position coordinates from the smartphone's integrated sensors. Post processing produced the resultant vertical acceleration for any sensor orientation and the corresponding RIF-index for a specified length of the segment (*21*). The operator manually initiated data logging near the instant that the vehicle crossed the duct tape. Consequently, the latency of achieving GPS lock resulted in some sections not completely overlapping the IRI sections characterized. Nevertheless, analysis of the data revealed that sections of 210-meters (689-ft) near the centers of each test site provided the maximum overlap for all traversals.

The sedan used to collect the data that produce RIF-indices was a 2000 Toyota Camry. Hence, the PAVVET app converted both the sedan and the inertial profiler van to connected vehicles. The mounted orientation for the smartphone was vertical so that the operator could verify its operation and initiate data logging by tapping the screen (Figure 2c). This mount apparatus produced some spurious vibration modes due to the levered design of its base. However, a 21-tap finite impulse response (FIR) low-pass filter with cutoff frequency of 20 Hz adequately removed the noise and isolated the quarter-car sprung- and unsprung-mass modes needed to produce the RIF-indices. The signal-processing algorithm of the RIF-transform also removes any offset in the resultant vertical acceleration to ignore static g-forces from earth's gravity. The maximum update rate achieved for the inertial sensors of the smartphone was approximately 93 Hz. Previous studies recommended that agencies standardize the inertial sample rate and the sensor mount apparatus to improve the precision of measurements with fewer traversal samples (*6*). The update rate achievable from the integrated GPS receiver of the smartphone was 1 Hz. Therefore, the data processing algorithm interpolated the distance between inertial samples by using the instantaneous velocity and sample time increments. The inertial navigation output of the GPS receiver produced the velocity signal.

Experimental Results

The data from the three sets of traversals (Table 1) include parameters from the inertial profiler traversals at approximately 45 and 60 MPH, and the sedan traversals at approximately 45 MPH. As expected, the EAR/IRI ratios for each vehicle and traversal speed agree in their relative change, albeit slight, across test sites (Figure 3). As Equation (3) suggests, the higher speed traversals of the inertial profiler produce expectedly larger EAR-indices. Hence, the EAR/IRI ratios are consistently higher. The EAR-indices from the sedan are consistently lower than the corresponding indices from the inertial profiler because the VIF of the former generally provides greater isolation from road roughness than the latter.

As described previously, the IRI does not reflect variations in the actual vehicle velocity and suspension response whereas the RIF-indices do. Hence, with only 7 to 9 traversals available

per test site the MOE_{95} for the RIF-indices were greater than the corresponding IRI values as expected. The average MOE_{95} for the RIF-indices and the IRI derived from the inertial profiler was approximately 10% and 3.5%, respectively. With more traversals available, the MOE_{95} for the RIF-indices derived from the sedan averaged approximately 4%, which is comparable to the MOE_{95} obtained for the IRI. From Equation (12), the average proportional impact of the velocity variance to the precision dilution of RIF-indices was approximately 3% and 1.5% for the inertial profiler traversals at 45 MPH and 60 MPH, respectively. Expectedly, the sedan traversals contributed a slightly higher average velocity variance of approximately 5% to dilute the precision of RIF-indices.

Convergence of RIF/IRI Proportionality

The law of large numbers in probability theory dictates that the average value from many trials will converge to the expected value (*24*).This section demonstrates that the probability distribution of the RIF/IRI ratios follows the well-established t-distribution that is appropriate for data sets smaller than 30 samples. Therefore, the RIF/IRI proportionality must converge to a mean value with increasing levels of precision as the traversal volumes from connected vehicles increase beyond 30. This guaranteed convergence in connected vehicle environments obviates the need to calibrate the RIF/IRI ratio for individual vehicles. The histograms of the RIF/IRI ratios for the test traversals conducted using the inertial profiler at two different speeds, and the sedan at the lower speed demonstrate this agreement with the classical distribution (Figure 4). The critical chi-squared values (Equation 8) are substantially smaller than the chi-squared distribution evaluated at 5% significance (Table 2). That is, the average significance is approximately 86%, which is much greater than 5%. Therefore, the tests cannot reject a hypothesis that the distribution of the ratios follows the t-distribution.

The strong agreement with the classic distribution indicates that additional vehicle traversals will further increase the precision of estimating the IRI from connected vehicle data. This fact is evident from the sedan traversals that produced 69 samples. In particular, the average MOE_{95} for the RIF/IRI ratios obtained using the inertial profiler at each speed is approximately 6% with 22 to 23 samples. In contrast, the MOE_{95} obtained using the sedan approaches 2% after 69 samples aggregated across the three test sites.

Plotting the MOE_{95} calculated after including data from each additional traversal exemplifies the diminishing error trend (Figure 5). The exponential trend of decline is similar for the data obtained using the inertial profiler (IP) wagon at two speeds and the sedan at 45 MPH. Extrapolating the trend based on the model indicated suggests that the precision will improve such that the MOE_{95} will diminish beyond 5% and 2% as the number of traversals exceeds 30 and 80, respectively. The model for these case studies has a decay exponent of -0.9, which is greater than the theoretical floor of -0.5 established in Equation (9). The coefficient of determination (R^2) for the model is nearly unity, indicating near perfect goodness-of-fit with the data.

The Annual Average Daily Traffic (AADT) volume medians are 23,000 and 82,000 passenger cars per lane for rural and urban interstate facilities, respectively (*26*). Therefore, as connected vehicle environments mature, or as more travelers use apps similar to PAVVET, the MOE_{95} will become negligible within one hour of data collection.

SUMMARY AND CONCLUSIONS

The methods and models validated in this research breaks through long-standing constraints to reduce the cost, expand the reach, and increase the frequency of ride quality characterizations. The technique leverages the large volume of sensor data expected from connected vehicles to produce a consistent characterization of roughness that represents the average ride quality for any facility. The case studies of this research utilized a certified and calibrated inertial profiler and a regular passenger vehicle and found that the margin-of-error will diminish below 5% and 2% after 30 and 80 traversals, respectively. International standards for vibration safety result in a high consistency of suspension system performance to suppress roughness that produces human discomfort in a specific frequency range. Such safety standards preclude large variations in vehicle suspension responses, regardless of the vehicle size and weight; the IRI relies on this fact. Consequently, guidelines for the consistent performance of suspension systems place practically achievable bounds on the number of traversals that will produce an accurate and high-precision characterization of the true ride quality that any facility provides.

The case studies conducted for this research demonstrated that the direct proportionality relationship with the IRI remains consistent across facilities that exhibit different levels of roughness. Therefore, the direct proportionality of the connected vehicle method at fixed speeds will extend investments in IRI datasets through simple scaling. Agencies have the flexibility of continuing use of the IRI while expanding applications that utilize the RIF- and TWIT-indices. Unlike the IRI, the computational simplicity of the RIF-transform in producing the EAR and TWIT indices enables low-power mobile devices such as smartphones to compute them directly for real-time observation and reporting. Their computational simplicity minimizes the cost of adoption worldwide.

The connected vehicle approach addresses the IRI utility gaps by extending their application to all facility types, and at all speeds. The fixed quarter-car model and fixed speed simulation of the IRI accounts for its spatial wavelength bias. Conversely, the inertial sensors that all vehicles already integrate will directly reflect the actual roughness that riders experience. The TWIT precludes wavelength biases by integrating roughness induced at all speeds that vehicles use the facility. Moreover, characterizing ride quality by averaging the roughness indices from large traversal volumes produce a more statistically significant measure of the ride quality that users actually experience. That is, sampling the inertial response of vehicles that use every facility provides a more complete characterization of the roadway network and its present ability to serve the traveling public. Furthermore, the accuracy and precision of applications that forecast pavement deterioration and localize anomalies will improve continuously with higher data volume as more connected vehicles participate.

The connected vehicle approach of this study has a broad reach. It will enable cost-reduced, continuous situational awareness and objective asset management for all roads across the globe. Nations that cannot afford modern profiling equipment to produce the IRI will have a substantially lower cost alternative by using smartphones to enable connected vehicles that are compatible with their communications infrastructure. Agencies that utilize the TWIT with GIS tools to visualize roughness will enhance their decision support capabilities and reduce personnel training needs to interpret roadway performance data. By integrating the models presented in this research into scalable software platforms that incorporate custom maintenance rules, agencies throughout the world will be able to realize substantial savings by making effective data-driven decisions to optimize their roadway asset preservation practices. Future research will examine

applications of the RIF-transform to establish rules for maintenance decision support for different facility types and under different environmental and usage considerations.

ACKNOWLEDGEMENTS
A grant from the Mountain Plains Consortium supported this research.

REFERENCES

1. Bridgelall, R. Connected Vehicle Approach for Pavement Roughness Evaluation. *Journal of Infrastructure Systems*, Vol. 20, No. 1, 2014, pp. 1-6.
2. Besinger, F. H., D. Cebon, and D. J. Cole. Force Control of a Semi-Active Damper. *Vehicle System Dynamics: International Journal of Vehicle Mechanics and Mobility*, Vol. 24, No. 9, 1995, pp. 695-723.
3. Griffin, M. J. *Handbook of Human Vibration*. Elsevier, New York, 1990.
4. Jazar, R. N. *Vehicle Dynamics: Theory and Applications*. Springer, New York, 2008.
5. *Smoothness Specifications Online - Overview of Current Practices*. The Transtec Group, Inc., March 28, 2012. SmoothPavements.com. Accessed March, 28 2015.
6. Bridgelall, R. Inertial Sensor Sample Rate Selection for Ride Quality Measures. *Journal of Infrastructure Systems*, Vol. 21, No. 2, 2015, pp. 04014039 (1-5).
7. Performance Analysis Via Vehicle Electronic Telemetry (PAVVET). Upper Great Plains Transportation Institute, December 9, 2014. www.ugpti.org/smartse. Accessed March, 28 2015.
8. *Measuring, Characterizing, and Reporting Pavement Roughness of Low-Speed and Urban Roads*. NCHRP 10-93, Transportation Research Board of the National Academies, Washington, D.C., 2013.
9. *Transportation Statistics Annual Report 2013*. Bureau of Transportation Statistics, U.S. Department of Transportation, 2014.
10. Merritt, D. K., G. K. Chang, and J. L. Rutledge. *Best Practices for Achieving and Measuring Pavement Smoothness, A Synthesis of State-of-Practice*. Louisiana Transportation Research Center, Baton Rough, Louisiana, 2014.
11. Ahlin, K., and N. J. Granlund. Relating Road Roughness and Vehicle Speeds to Human Whole Body Vibration and Exposure Limits. *International Journal of Pavement Engineering*, Vol. 3, No. 4, 2002, pp. 207-216.
12. Papagiannakis, A. T. The Need for a New Pavement Roughness Index; RIDE. In *International Truck & Bus Meeting & Exposition*, Washington, D.C., 1997.
13. Lak, M. A., G. Degrande, and G. Lombaert. The Influence of the Pavement Type on Ground-borne Vibrations Due to Road Traffic. *In Proceedings of the 8th International Conference on Structural Dynamics*, Leuven, Belgium, 2011.
14. Ramji, K., A. Gupta, V. H. Saran, V. K. Goel, and V. Kumar. Road Roughness Measurements using PSD Approach. *Journal of the Institution of Engineers, Civil Engineering Division*, Vol. 85, 2004, pp. 193-201.
15. Walker, R. S., E. Fernando, and Y. Sho. *A Methodology for Bump Detection Using Inertial Profile Measurements*. The University of Texas at Arlington for TxDOT, Arlington, Texas, 2005.
16. Loizos A., and C. Plati. An Alternative Approach to Pavement Roughness Evaluation. *International Journal of Pavement Engineering*, Vol. 9, No. 1, 2008, pp. 69-78.

17. Múčka, P., and J. Granlund. Comparison of Longitudinal Unevenness of Old and Repaired Highway Lanes. *Journal of Transportation Engineering*, Vol. 138, No. 3, 2012, pp. 371-380.
18. Gillespie, T. D., M. W. Sayers and C. A. V. Queiroz. *The International Road Roughness Experiment: Establishing Correlation and Calibration Standard for Measurement*. The World Bank, Washington, D.C., 1986.
19. Dawkins, J., D. Bevly, B. Powell and R. Bishop. *Investigation of Pavement Maintenance Applications of Intellidrive*. University of Virginia, Charlottesville, Virginia, 2011.
20. Du, Y., C. Liu, D. Wu and S. Jiang. Measurement of International Roughness Index by Using Z-Axis Accelerometers and GPS. *Mathematical Problems in Engineering*, 2014, p. 928980 (1-10).
21. Bridgelall, R. A Participatory Sensing Approach to Characterize Ride Quality. In *Proceedings of SPIE Volume 9061, Sensors and Smart Structures Technologies for Civil, Mechanical, and Aerospace Systems*, Bellingham, Washington, 2014.
22. Bridgelall, R. Precision Bounds of Pavement Deterioration Forecasts from Connected Vehicles. *Journal of Infrastructure Systems*, Vol. 21, No. 1, 2015, pp. 04014033 (1-7).
23. Agresti A., and B. Finlay. *Statistical Methods for the Social Sciences*, 4th ed., Pearson, New York, 2008.
24. Papoulis, A. *Probalility, Random Variables, and Stochastic Processes*. McGraw-Hill, New York, 1991.
25. Perera R. W., and G. E. Elkins. *LTPP Manual for Profile Measurements and Processing. FHWA*, U.S. Department of Transportation, 2013.
26. Highway Functional Classification: Concepts, Criteria and Procedures. FHWA, U.S. Department of Transportation, 2013.

TABLE 1 Summary Traversal Parameters

Inertial Profiler at 45 MPH										
Site	N_v	$\overline{R}_{45}^{689}$	**MOE$_{95(EAR)}$**	I_{45}^{1000}	**MOE$_{95(IRI)}$**	RIF/IRI	$\overline{\overline{v}}$	$\sigma_{\bar{v}}$	$\overline{E}_{gz}^{L}$ (μJ)	η_{vR}^{L}
1	7	0.225	9.5%	1.354	2.7%	0.17	43	0.8	136.4	3.1%
2	8	0.177	13.6%	0.939	1.6%	0.19	43	0.8	85.0	1.3%
3	8	0.168	7.4%	0.901	1.6%	0.19	43	0.8	75.8	4.9%
Inertial Profiler at 60 MPH										
Site	N_v	$\overline{R}_{60}^{689}$	**MOE$_{95(EAR)}$**	I_{60}^{1000}	**MOE$_{95(IRI)}$**	RIF/IRI	$\overline{\overline{v}}$	$\sigma_{\bar{v}}$	$\overline{E}_{gz}^{L}$ (μJ)	η_{vR}^{L}
1	8	0.275	9.4%	1.348	9.9%	0.20	57	0.8	115.8	3.1%
2	9	0.202	14.2%	0.955	2.5%	0.21	57	0.8	63.9	0.8%
3	9	0.208	7.2%	0.906	2.5%	0.23	58	0.5	65.6	1.0%
Sedan at 45 MPH										
Site	N_v	$\overline{R}_{45}^{689}$	**MOE$_{95(EAR)}$**			RIF/IRI	$\overline{\overline{v}}$	$\sigma_{\bar{v}}$	$\overline{E}_{gz}^{L}$ (μJ)	η_{vR}^{L}
1	23	0.141	4.8%			0.10	45	0.9	50.1	3.2%
2	23	0.098	3.8%			0.10	45	0.9	24.0	5.1%
3	23	0.103	3.2%			0.11	45	0.9	26.3	7.1%

TABLE 2 Summary of Chi-Squared Testing

	Inertial Profiler		**Sedan**
Student-t	45 MPH	60 MPH	45 MPH
df	2	2	5
χ^2 (α = 5%)	6.0	6.0	6.0
χ^2 Data	0.4	0.5	0.6
Significance α (%)	**81.5**	**77.4**	**98.6**
Amplitude	0.6	0.8	0.5
Mean	0.178	0.208	0.107
Standard Dev.	0.024	0.044	0.010
Samples	23	22	69
RIF/IRI Mean	0.181	0.218	0.107
RIF/IRI Standard Deviation	0.025	0.030	0.011
MOE$_{0.95}$ (%)	5.9	6.1	2.4

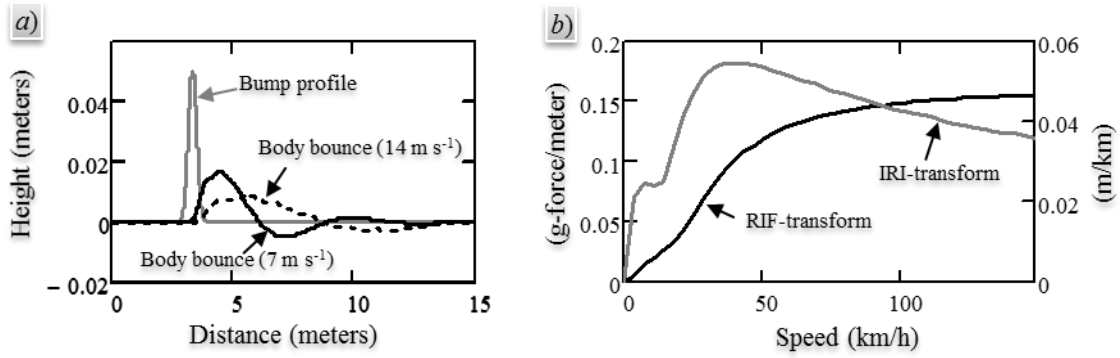

FIGURE 1 RIF- and IRI-transforms from a simulated bump traversal.

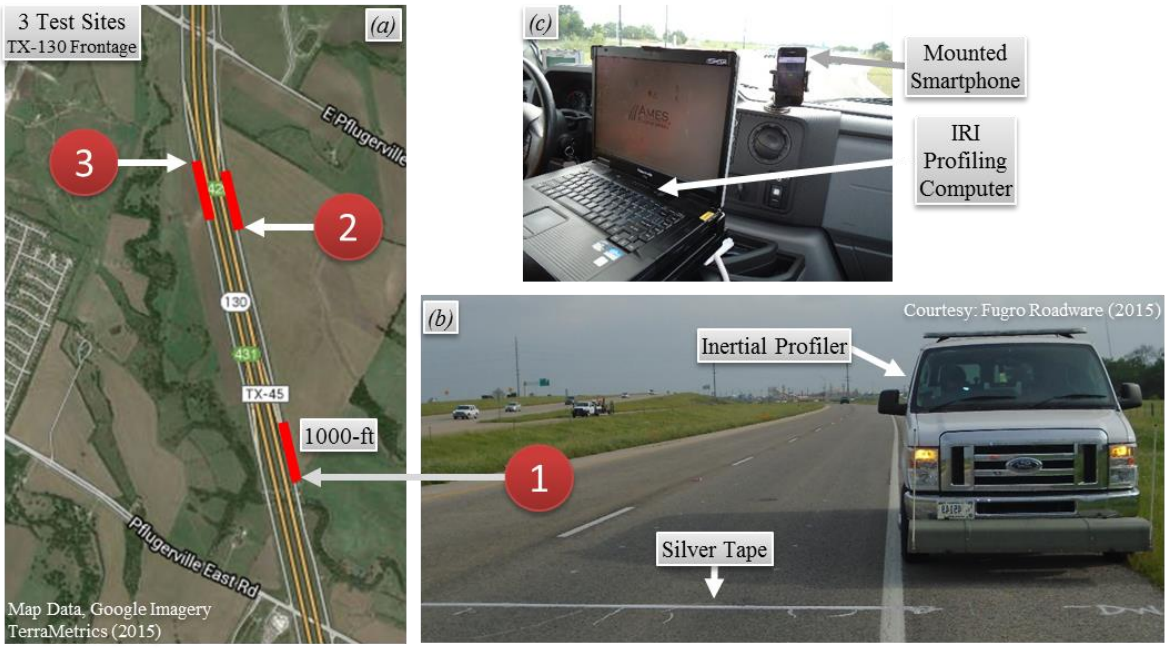

FIGURE 2 The roadway sections analyzed.

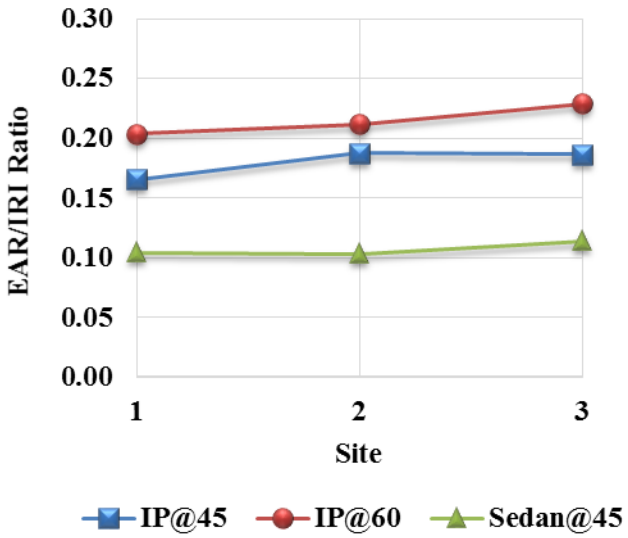

FIGURE 3 EAR and IRI roughness indices for each test site.

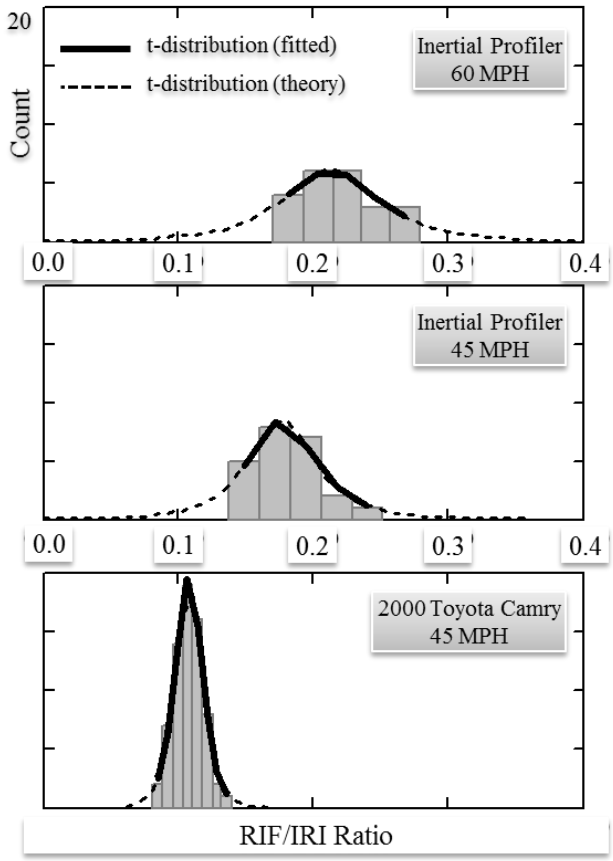

FIGURE 4 Distribution of RIF/IRI ratios at each traversal speed.

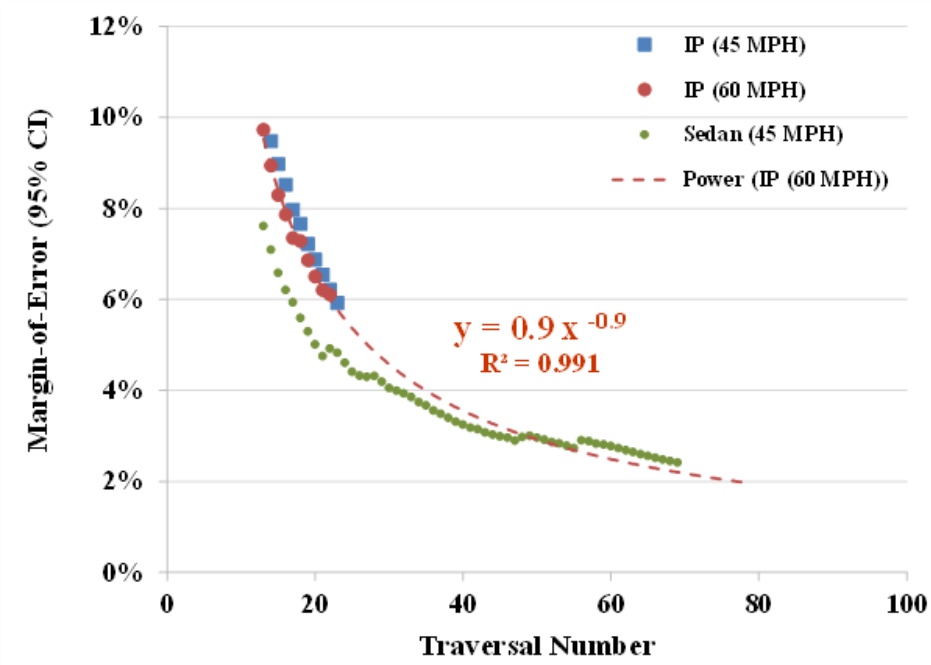

FIGURE 5 Margin-of-error trend for the RIF/IRI ratios.